Magic Number Pt$_{13}$ and Misshapen Pt$_{12}$ Clusters: Which One is the Better Catalyst?

Takane Imaoka,[†] Hirokazu Kitazawa,[†] Wang-Jae Chun,[‡] Saori Omura,[†] Ken Albrecht,[†] and Kimihisa Yamamoto*,[†]

[†]Chemical Resources Laboratory, Tokyo Institute of Technology, Yokohama 226-8503, Japan
[‡]Graduate School of Arts and Sciences, International Christian University, Mitaka, Tokyo 181-8585, Japan

S *Supporting Information*

ABSTRACT: A relationship between the size of metal particles and their catalytic activity has been established over a nanometer scale (2−10 nm). However, application on a subnanometer scale (0.5−2 nm) is difficult, a possible reason being that the activity no longer relies on the size but rather the geometric structure as a cluster (or superatomic) compound. We now report that the catalytic activity for the oxygen reduction reaction (ORR) significantly increased when only one atom was removed from a magic number cluster composed of 13-platinum atoms (Pt$_{13}$). The synthesis with an atomic-level precision was successfully achieved by using a dendrimer ligand as the macromolecular template strictly defining the number of metal atoms. It was quite surprising that the Pt$_{12}$ cluster exhibited more than 2-fold catalytic activity compared with that of the Pt$_{13}$ cluster. ESI-TOF-mass and EXAFS analyses provided information about the structures. These analyses suggested that the Pt$_{12}$ has a deformed coordination, while the Pt$_{13}$ has a well-known icosahedral atomic coordination as part of the stable cluster series. Theoretical analyses based on density functional theory (DFT) also supported this idea. The present results suggest potential activity of the metastable clusters although they have been "missing" species in conventional statistical synthesis.
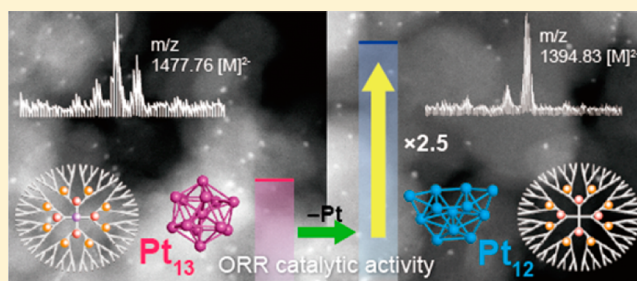
INTRODUCTION

Metal nanoparticles are extensively used as catalysts or for gas storage because they provide excellent performance together with a reduced requirement for precious elements such as Pt, Rh, or Pd.[1] Platinum particles are especially important for fuel cell technology. However, it is believed in the fuel-cell community that smaller platinum particles (<2 nm) are not suitable for oxygen reduction reaction (ORR) catalysis.[2,3] On the basis of this simple idea, platinum nanoparticles are thought to be at the limit of their catalytic performance. Despite this common notion, some researchers and us reported that much smaller particles (clusters) have a better catalytic performance for the ORR.[4,5] Such contradictory claims suggest that the catalytic activity no longer depends on the particle size but on other factors. To design more catalytically active nanoparticles, a deeper insight into the particles with respect to their structure and properties is very important. To date, three different approaches have been employed to synthesize these small nanoparticles. (1) A conventional methods from metal ions with appropriate supporting materials, surfactants, or polymer bonds through a solution-phase reduction or the solvothermal direct synthesis of nanoparticles are widely used for various applications.[6,7] In principle, this procedure is inevitably accompanied by a considerable polydispersity in the number of atom elements composing each particle. (2) The mass-selected cluster approach by gas-phase synthesis enables a perfect monodispersity in the number of atoms.[8] However, the available amount of the clusters is far below the requirement of the catalytic applications. (3) The ligand-assisted approach occasionally produces ultrafine metal clusters with a completely defined structure in a solution.[9,10] However, this method strongly depends on the inherent stability of special clusters (often called magic-number clusters). In addition, such a ligand-protected cluster has lost its catalytic activity because the active surface is almost completely covered.

In contrast, a template approach using a discrete macro-molecular ligand is effective for the preparation of size-controlled nanoparticle catalysts.[11] Especially, phenylazomethine dendrimer ligands as an improved template allow one to define an unambiguous number of atoms in one particle (cluster)[5,12] because the dendrimer can precisely assemble metal ions by controlling their molecular-level formula based on a stoichiometric adjustment.[13] This synthetic breakthrough has provided a significant advantage in that the number of the metal atoms can be preprogrammed by the dendrimer structure and the metal/dendrimer stoichiometry regardless of the resulting cluster stability. By this approach, we can obtain a novel cluster composition even if it deviated from the stable magic number.
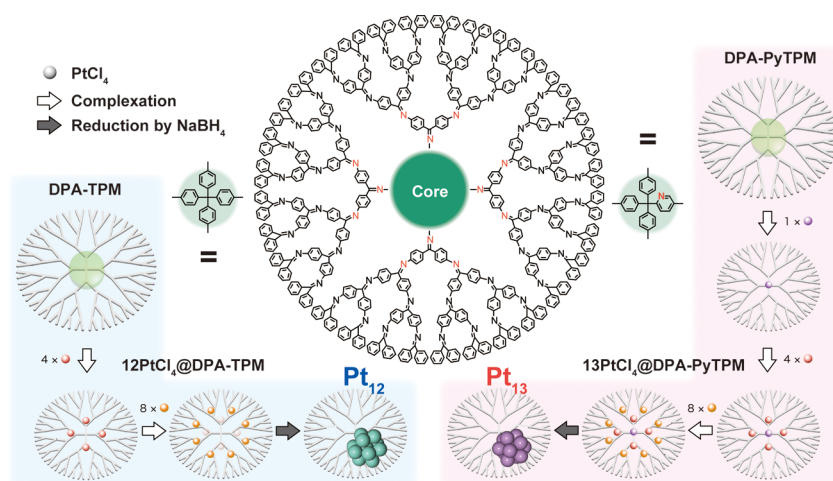
Figure 1. Schematic representation of the size-selective synthesis of platinum clusters. DPA-TPM and DPA-PyTPM were used as the template ligands for Pt$_{12}$ and Pt$_{13}$ clusters, respectively.

Previous investigations of cluster catalysts all assumed a stable series such as that based on the topological magic number structure (e.g., Pt$_{13}$, Pt$_{55}$...) with high symmetry.[3] Therefore, how different is the activity between the symmetric stable clusters and misshapen nonmagic number clusters? We can now access both clusters by the robust template approach. For example, our previous result of an ultrafine Pt$_{12}$ cluster exhibiting an exceptionally high performance would be a suitable research target to understand the real ORR activity of the platinum clusters.[5] We have also prepared a Pt$_{13}$, which is known to be a stable magic number cluster. Comparing these two clusters with respect to the structure and catalysis would provide the origin of the high catalytic performance of platinum clusters and some important knowledge to find other missing "hot" nanoparticles.

■ EXPERIMENTAL SECTION

Synthesis of Pt$_{12}$. To a solution (3 μmol L^{-1}, 1 mL) of DPA-TPM (fourth-generation dendritic phenylazomethine with a tetraphenyl-methane core)[14] in a dehydrated mixed solvent (chloroform/acetonitrile = 1/1) was added a platinum chloride (3 mmol L^{-1}, 12 μL) solution in dehydrated acetonitrile. The mixture was stirred for 1 h to complete the complexation under a dry nitrogen atmosphere. A 10 μL aliquot of a freshly dissolved NaBH$_4$ solution (10 mg in 1 mL of methanol) with H$_2$ gas evolution was then quickly added to a stirred solution of the complex. The resulting solution containing the Pt$_{12}$ cluster after a slight color change was used for the experiments. Because the cluster without any stabilization by a support easily aggregates, the solution should be used as quickly as possible.

Synthesis of Pt$_{13}$. To a solution (3 μmol L^{-1}, 1 mL) of DPA-PyTPM (fourth-generation dendritic phenylazomethine with a triphenylpyridylmethane core)[15] in a dehydrated mixed solvent (chloroform/acetonitrile = 1/1) was added a platinum chloride (3 mmol L^{-1}, 13 μL) solution in dehydrated acetonitrile. The following procedure is the same as the preparation of the Pt$_{12}$ cluster.

Determination of the Cluster by ESI-TOF-MS. To a resulting solution of Pt$_{12}$ or Pt$_{13}$, pure carbon monooxide gas (atmospheric pressure) was introduced and stirred for 3 min. The filtered solution was then quickly injected into a mass spectrometer (Bruker, micrOTOF II or Waters, LCT Premier) through a syringe pump at the flow rate of 10 μL s^{-1}. The spectra were measured in the negative-ion mode, which was calibrated with an ESI-L Low Concentration Tuning Mix (Agilent Technologies Co.). To modulate the fragmentation of the carbonyl (CO) ligands, we adjusted the capillary-exit voltage (Bruker) or the cone voltage (Waters). The dry

gas flow rate and other miscellaneous parameters were adjusted to maximize the intensity of the target ion peaks.

XAFS Data Acquisition. XAFS was measured in transmission mode at the BL12C at the Photon Factory of the Institute of Material Structure Science, National Laboratory for High Energy Physics (KEK-IMSS-PF, Tsukuba, Japan). The electron storage ring was operated at 2.5 GeV−400 mA. Synchrotron radiation from the storage ring was monochromatized with Si (111) channel-cut crystals. Ionization chambers filled with Ar(15%)−N$_2$(85%) mixed gas and Ar were used as detectors monitoring incident X-rays (I_0) and transmitted X-rays (I), respectively. The angle of the monochromator was calibrated by using Pt foil, the inflection point of which at the edge was set at 11558.2 eV. To reduce the correlation between coordination numbers and the Debye−Waller factor, all measurements were carried out at 30 K. Curve-fitting analysis was carried out as described in Supporting Information.

The platinum cluster samples supported on carbon powder were prepared as follows. To the resulting solution of Pt$_{12}$ or Pt$_{13}$ was added graphitic mesoporous carbon powder (Aldrich). The amount of mesoporous carbon was adjusted to 1.0 weight% of the platinum loaded on the carbon materials. The suspensions were then stirred for 10 min followed by an ultrasonic process for 30 min. Finally, each powder as carbon-supported platinum clusters was obtained by filtrations of the suspension. Most of the platinum clusters should be supported on the carbon because no significant amount of the platinum was detected in the filtrate.

Electrochemical Measurements. Electrochemical measurements were performed by a multipurpose electrochemical workstation (ALS-750b, CH Instruments). A glassy carbon disk electrode (∅ 6.0 mm) was used as the working electrode. The electrode surface was polished with diamond and alumina paste and then rinsed in methanol with ultrasonication prior to use. An Ag/AgCl electrode in 3 mol L^{-1} NaCl$_{aq}$ and a platinum coil were used as the quasireference and counter electrodes, respectively. Cyclic voltammetry (CV) and rotating disk voltammetry (RDV) measurements were carried out in an aqueous HClO$_4$ solution (0.1 mol L^{-1}), which was thoroughly bubbled with O$_2$ or N$_2$ gas prior to the measurements. During the measurements, the atmospheric conditions were kept constant with flowing O$_2$ or N$_2$ gas. For each cluster sample, the solution was cast on the electrode and then dried under vacuum. The variation in the amount of the solution was 1−10 μL. The weight of the platinum element on the electrode was calculated from the concentration and the volume used for the casting. The kinetic limiting current density was calculated using the Koutecky−Levich equation as previously reported.[5]

DFT Calculations. All DFT calculations were performed using a DMol3 module within Material Studio 6.0 (Accerlys). The GGA-RPBE functional for the exchange and correlation was used. The DNP

3.5 (double numerical and polarization basis set provided with the Material Studio) was employed as the basis set. We used preset values defined as the "fine" option for the integration accuracy, SCF tolerance, and orbital cutoff quality. The core electrons were treated as effective core potentials. Each cluster model was optimized by minimizing the energy by the DFT calculation. The oxygen binding energies were calculated on each 3-fold hollow site on the surface of the resulting Pt cluster model. The O atom was always kept at a distance of 2.07 Å from the three neighboring Pt atoms without the geometry optimization.

General. HAADF-STEM images were collected using a transmission electron microscope (JEOL, JEM-2100F). The supported clusters (Pt_{12} or Pt_{13}) were deposited on an elastic carbon film with a Cu mesh (Nisshin EM Co.). X-ray photoelectron spectra (XPS) were obtained using an instrument (Ulvac-phi, ESCA1700R) with Mg Kα radiation. For the XPS measurement, gold powder was deposited on a glassy carbon substrate (Tokai Carbon Co., Ltd.) as the internal reference with the cluster sample, and the Au $4f_{7/2}$ (83.8 eV) peak was used to offset the electron binding energy.

■ RESULTS

Catalytic Activity. The Pt_{13} cluster was synthesized using a dendrimer having a pyridyl-triphenylmethane core (DPA-PyTPM)[15] as a special template suitable for the synthesis of Pt_{13} via a similar procedure for the Pt_{12} cluster.[5] Chemical reduction by sodium borohydride ($NaBH_4$) quickly afforded the resulting cluster compound (Pt_{12} and Pt_{13}) from the corresponding precursor as metal complexes ($12PtCl_4$@DPA-TPM and $13PtCl_4$@DPA-pyTPM) of platinum tetrachloride (Figure 1). The as-synthesized clusters in solution were promptly cast on glassy carbon electrodes (GCE) used for the electrochemical analysis to clarify the amount of the modified platinum species. The perfect removal of NaCl or boron compounds by simple rinsing with water was not proven. Instead, we synthesized these two cluster catalysts (Pt_{12} and Pt_{13}) using the same amount of reducing agent under the same conditions. The reproducibility was carefully checked to eliminate the effect by unexpected impurities. Therefore, these impurities might have the same effect on each cluster. The oxygen reduction reaction (ORR) catalytic activity of these clusters was obtained as the kinetic-limiting current values by rotating disk voltammetry (RDV) measurement using the modified GCE together with the calculation by the Koutecky–Levich equation (Figure S1, Supporting Information).[5] A minimum amount of the platinum catalyst was modified (max. 30 ng on the GCE) because the observed catalytic current should be significantly below the diffusion limit to clarify the kinetic limit. The slope of the relationship between the kinetic current and amount of the modified platinum indicated the mass activities of Pt_{12} and Pt_{13}. Unexpectedly, the Pt_{12} cluster exhibited more than a 2-fold mass activity of the Pt_{13} cluster even though the difference in the number of platinum atoms is only 1 (Figure 2). The possible fractions of the surface atoms for Pt_{12} and Pt_{13} are both at least 92%. This idea suggests that the contribution by the surface area fraction is negligible. Thus, the result indicates a significant transition in the property from Pt_{13} to Pt_{12}, which might induce changes in the geometry or characteristics of the active sites. As described in a previous report,[5] Pt_{12} has a higher mass activity than Pt_{28} and Pt_{60}. Meanwhile, Pt_{13} exhibited a catalytic activity lower than that of the larger ones. These contrasting observations suggest that the catalytic activity no longer depends on the size of the clusters but rather the specific structures for the given number of metal atoms.
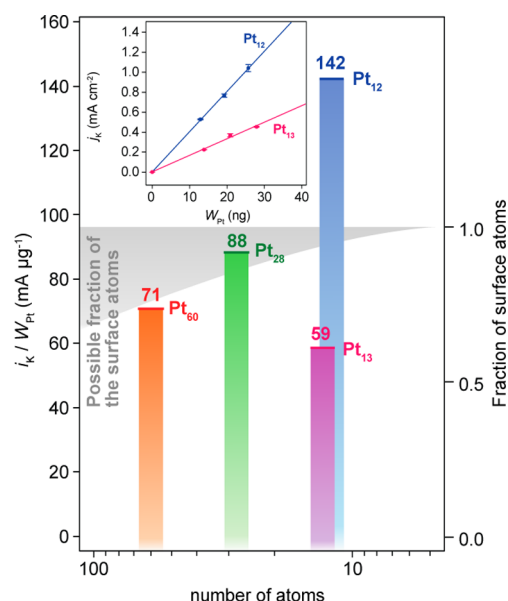

Figure 2. ORR catalytic activities of platinum clusters (Pt_{12} and Pt_{13}). ORR mass activities of the clusters having a different number of platinum atoms. Pt_{12} and Pt_{13} significantly deviated from the expected values based on an increase in the surface fraction. (Inset) Kinetic current densities of Pt_{12} and Pt_{13} calculated using the Koutecky–Levich equation for different amounts of clusters modified on the electrode.

Confirmations of One-Atom Controlled Clusters. In the present case, the size of these clusters could be confirmed by HAADF-STEM (Figure 3).[16] However, the difference
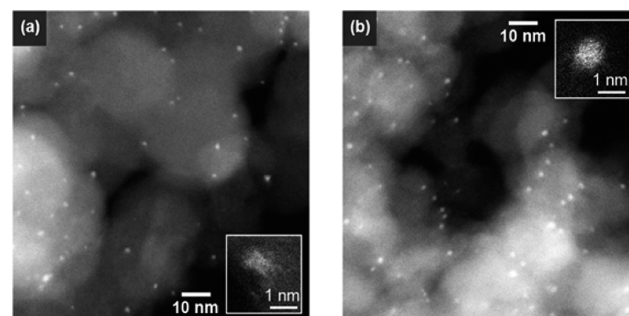

Figure 3. HAADF-STEM images of clusters. (a) Pt_{12} and (b) Pt_{13} supported on mesoporous carbon (1 wt % Pt). Inset pictures are the high magnification images of each focused cluster.

between the size of Pt_{12} and Pt_{13} clusters was too small to discuss. On the contrary, mass spectrometry is suitable to obtain direct evidence about the number of metal atoms because the clusters were almost monodisperse.[17] We attempted a ligand-exchange approach[18] to detect the clusters with tightly binding surface molecules. This trial was successful when we employed carbon monoxide (CO) as the ligand. Just after the synthesis of the platinum clusters (Pt_{12} or Pt_{13}) under a nitrogen atmosphere, pure carbon monooxide gas (1 atm) was quickly introduced to the reaction vessel and then stirred for 3 min at room temperature. The resulting mixture was expeditiously injected into an ESI-TOF-MS for the negative-ion measurement. As previously reported,[19] reconstructions of the cluster core were observed in our experiment, producing Chini-type cluster ions ($[Pt_{12}(CO)_{24}]^{2-}$) within several minutes after

the gas substitution.[20] Therefore, we conducted the sampling of the ligand-exchanged clusters with the least dead time and ignored the small amount of reconstructed species as the Chini-type cluster at m/z = 1506. The most intense peak was found at m/z = 1394.83 (negative mode) for the Pt_{12} cluster accompanying many isotope peaks all with 0.5 Da intervals, typical of divalent anion clusters (Figure 4). This spectrum was
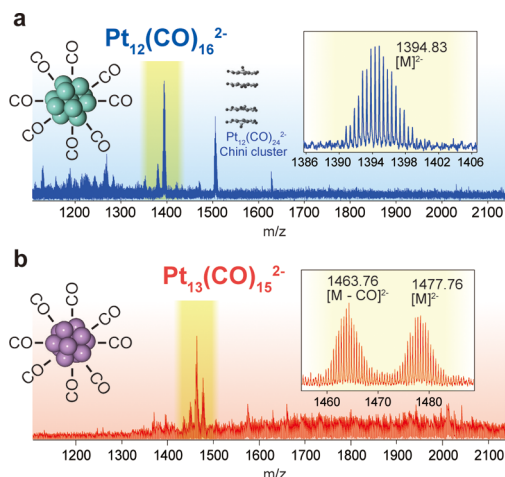

Figure 4. Negative-mode ESI-TOF-MS of the ligand-exchanged carbonyl clusters. The spectra were taken with as-prepared cluster-containing solutions (chloroform/acetonitrile = 1/1) after exposure to CO gas (3 min). The clusters were detected as dianion species, which were determined by the isotope patterns shown in the inset figures. (a) Pt_{12}, (b) Pt_{13}.

Figure 5. XAFS spectra of Pt_{12}, Pt_{13} supported on mesoporous carbon (1 wt % Pt), and Pt foil (bulk). (a) Pt L_3-edge and (b) Pt L_2-edge XANES spectra. (c) k^3-weighted EXAFS. (d) Fourier transforms of the k^3-weighted EXAFS.

completely matched with the theoretical isotope pattern of the $[Pt_{12}(CO)_{16}]^{2-}$ cluster ion. When the capillary-exit voltage was increased, the intensities of the fragmentation peaks of the carbonyl (CO) ligands increased due to the higher collision energy during the flight in a low-vacuum chamber (Figure S3, Supporting Information).[21] For the Pt_{13} cluster, the typical peaks at m/z = 1477.76 were observed, which were attributed to $[Pt_{13}(CO)_{15}]^{2-}$. It should be noted that the number of cluster valence electrons (CVE) of ligand-saturating $[Pt_{13}(CO)_{15}]^{2-}$ is calculated to be 162, which completely agreed with the CVE of the previously reported icosahedral Pt_{13} cluster determined by a crystallographic analysis.[10] This number is also known as the typical CVE for various icosahedral gold clusters.[22,23] In the present case, the structure of the Pt_{13} cluster is, therefore, thought to be icosahedron, one of the most stable forms of magic number clusters. Interestingly, $[Pt_{12}(CO)_{16}]^{2-}$ has more carbonyl ligands than $[Pt_{13}(CO)_{15}]^{2-}$ despite the smaller number of metal atoms. This fact indicates a less symmetric structure of the Pt_{12} with a smaller number of internal Pt–Pt bonds.

Structural Analysis. While the ESI-TOF-MS analysis provides information about the entire structure (molecular weights and formulas), XAFS (XANES and EXAFS) reflects information about the valence electrons and local structure around the platinum atoms such as the Pt–Pt distances or coordination numbers.[24] For the transmission-mode measurement, we employed a mesoporous carbon as the support, to which a 1 wt %(Pt) amount of the clusters (Pt_{12} and Pt_{13}) was adsorbed just after the synthesis (Figure 5). These low-temperature measurements (30 K) were carried out at both the Pt L_3 (XANES and EXAFS) and Pt L_2 (XANES) edges.
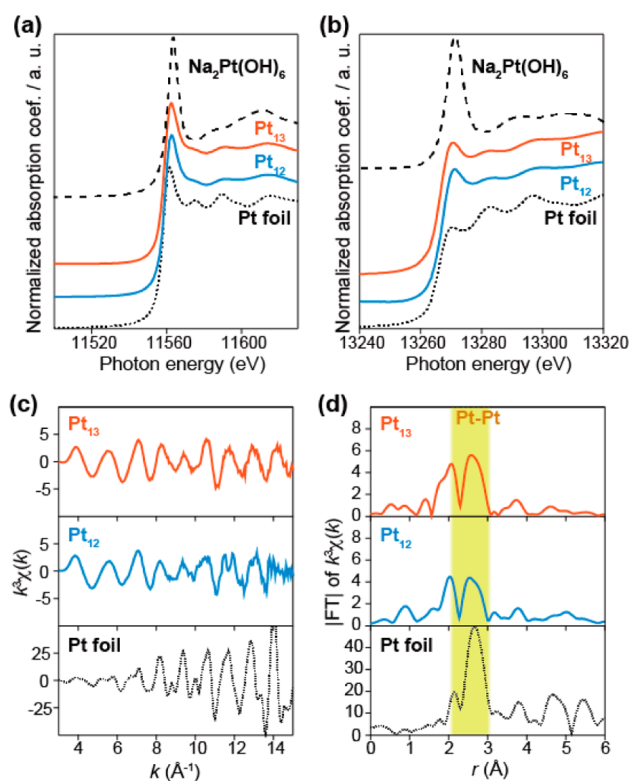
The XANES spectra were analyzed to evaluate both the electronic structure and the interaction between the clusters and dendrimers. The observed band structure of the Pt L_3 edge showed that both Pt_{12} and Pt_{13} clusters were similar to that of Pt foil except dampening in amplitude, which is a general trend of nanoclusters. Another feature is the peak top energies of the Pt clusters shifted only 0.9 eV to higher photon energy region. For oxidized Pt species such as $Na_2Pt(OH)_6$, the peak top energy is shifted to ~1.9 eV. In addition, white-line intensities at the edges are substantially weak relative to the oxidized species. Considering the energy resolution (0.5 eV) of XANES spectra, the clusters are thought to still be metallic but not oxidized. We assumed that the influence by the dendrimer coordination on electronic structures of the Pt clusters is not so considerable. Similar trends were also observed in the Pt L_2 edge. The calculated unoccupied d-electron states[24] were estimated to highlight the difference between two Pt clusters. We found that they were apparently electron deficient relative to Pt bulk, but no significant difference between the Pt clusters was observed. The X-ray photoelectron spectra (XPS) also showed the similarity at the Pt$4f_{7/2}$ peaks (Figure S2, Supporting Information).

In sharp contrast, the observed EXAFS spectra showed apparently different features. Noteworthy is that the oscillation amplitude of Pt_{12} is weaker than that of Pt_{13}. Another important feature is that the fine structures at around k = 8–10 Å^{-1} are not identical. It assumes that the local structures of the two clusters would be different. Curve-fitting results only by the first Pt–Pt shell (Table 1) provided reasonable coordination numbers (N) and interatomic distances (r). The observed N values of the Pt clusters agreed well with those estimated from

Table 1. Curve-Fitting Results for the EXAFS Data[a]

sample	bond	N^b	$r/Å^c$	$\Delta E_0/eV^d$	$\Delta\sigma^2/10^{-3}$ Å$^{2\,e}$	$R_f/\%^f$
Pt foil[g]	Pt−Pt	12	2.77	n/a	n/a	n/a
Pt$_{12}$	Pt−Pt	5.4 ± 0.9	2.74 ± 0.01	8.6 ± 2.1	8.5 ± 0.1	19.5
Pt$_{13}$	Pt−Pt	7.8 ± 1.2	2.74 ± 0.01	11.2 ± 1.8	9.8 ± 0.1	10.7

[a]Fourier transform region is limited for Δk = 3−15 Å^{-1}, Fourier filtering region is limited Δr = 1.75−3.04 Å for Pt$_{12}$, Δr = 1.65−3.04 Å for Pt$_{13}$. [b]Coordination number of the shell. [c]Interatomic distance. [d]Difference in the edge position. [e]Debye−Waller factor. [f]R_f factor. [g]Crystallographic data.
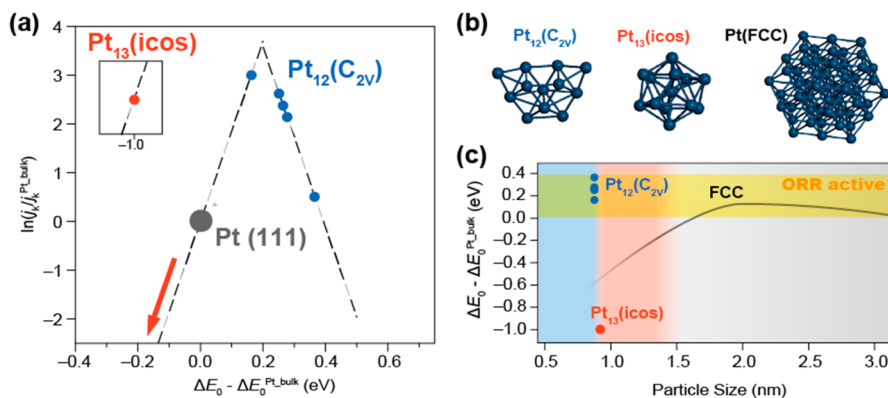

Figure 6. Volcano plots and free-energy diagrams for the oxygen reduction reaction by Pt catalyst. (a) Kinetic current density (j_K) plotted as a function of the calculated oxygen adsorption energy (ΔE_0). All data are shown relative to Pt. The volcano line (dash) and the plots (white circle) for the Pt-based transition metal alloys were from ref 31. The predicted j_K values based on the calculated ΔE_0 for each nonequivalent 3-fold hollow site on Pt$_{12}$(C$_{2v}$) were plotted as blue circles. The ΔE_0 values for Pt$_{13}$(icos) were out of the range (−1.0 eV) of this diagram. (b) Optimized geometric structures of Pt$_{12}$(C$_{2v}$), Pt$_{13}$(icos), and the FCC (face-centered cubic) nanoparticle assumed in this investigation. (c) A diagram of the relation between the particle size and the relative oxygen binding energy (ΔE_0).

the particle sizes.[25] Assuming the presence of light elements (we employed carbon atoms) near the surface platinum atoms, the qualities of the curve fitting (R_f values) were significantly improved (Table S2, Supporting Information). In this case, the coordination number (N) of Pt−Pt for the Pt$_{13}$ cluster is 6.5, which is in good agreement with the theoretical N from an icosahedral cluster model (N = 6.46). A contribution of Pt−N was not excluded because EXAFS cannot discriminate between the Pt−C and Pt−N bonds in the multiple X-ray absorption sites. The distances of 2.4−2.5 Å observed for the Pt−C (or Pt−N) contributions are too long to represent a direct bond formation. Alexeev et al. suggested the presence of similar long Pt−C contributions representing carbon atoms from a PAMAM dendrimer structure.[26] They have also suggested that the appearance of Pt−C contributions prevent Pt aggregation as a carbonaceous backbone.

Although the nearly monodisperse ESI-TOF-mass spectra for a number of platinum atoms were observed, these data do not warrant the 100% purity because it cannot deny the possibility of an invisible impurity. In contrast, EXAFS reflects all chemical compounds containing the target element, providing an averaged structural information if the samples were mixtures. The difference between Pt$_{12}$ and Pt$_{13}$ is indirect evidence of the narrow size distribution allowing investigation of the one-atom difference. If a greater size distribution unexpectedly exists, any difference in the property should not be observed. Actually, the expected number of assembling metal and its standard deviation is ca. 12 ± 1.3 for the metal-assembling phenyl-azomethine dendrimer (Figure S5, Supporting Information). With the size distribution, the experimentally determined difference (2.5-fold higher activity of Pt$_{12}$ against Pt$_{13}$) in the catalytic activities is considered as the minimum difference in the intrinsic activities.

Origin of the Catalytic Activity. A question now arises: What is the structure of Pt$_{12}$, and why is Pt$_{12}$ more catalytically active than Pt$_{13}$? To answer, several plausible structures of Pt$_{12}$ were investigated by DFT calculations. We examined several alternative structures of Pt$_{12}$ mostly derived from the literature (e.g., D_{3v}, D_{3h}, D_{5h}, C_{2v}, and two-dimensional clusters shown in the Supporting Information),[27] which were further optimized by the DFT calculations. Among these proposed models, the C_{2v}, D_{3h}, and D_{3v} structure showed relatively high stability, although they have atomic coordination significantly different from that of the icosahedral structure of Pt$_{13}$. For example, the coordination number (N) of the C_{2v} model is calculated to be 5.00, which is in good agreement with the experimental value (N = 5.2 when the Pt−C shell was assumed).

It is quite reasonable that Pt$_{12}$ has such a different atomic coordination from the icosahedral Pt$_{13}$ despite the small difference in the number of metal atoms. Removal of one platinum atom from the icosahedral Pt$_{13}$ necessarily forms a large pocket, which might destabilize the cluster. On the basis of this idea, a significant transition in the structure is expected. Previous studies of size-selected gas-phase gold clusters have also demonstrated that an increase in the number of gold atoms (n) in the cluster involves a significant transition in the structure at n = 12.[27] In our present study using ESI-TOF-MS, we have indeed observed evidence of the structural transition between n = 12 and 13. On the contrary, additional platinum attachments to the icosahedral Pt$_{13}$ do not induce any structural transition. We indeed observed the evidence of larger clusters (n = 14, ... 19) by ESI-TOF-MS when the equimolar amount of PtCl$_4$ for the dendrimer template (DPAG4-PyTPM) was set to more than 14 (PtCl$_4$ were overloaded). The numbers of carbonyl ligands accompanying Pt$_{13}$ and the larger clusters were all [n + 2] where n is the number of platinum atoms, indicating

that these larger clusters have a similar icosahedral-based structure (Figure S4, Supporting Information). For example, the number of CVEs for the observed $[Pt_{14}(CO)_{16}]^{2-}$, $[Pt_{15}(CO)_{17}]^{2-}$, and $[Pt_{16}(CO)_{18}]^{2-}$ are 174, 186, and 198, respectively. A 12CVE increase by each addition of one platinum atom can be interpreted as an attachment of the new platinum atom at the 3-fold hollow sites (in other words, face-sharing condensations with Pt_4 tetrahedra),[28] satisfying the Wade–Mingos $12n_s + 18$ rule (n_s is the number of atoms appearing as the shell).[23] This condensation may lead to the known Pt_{17}[29] or Pt_{19}[10] cluster having 210- or 232CVE, respectively.

However, the number of ligands on the Pt_{12} cluster was $[n + 4]$, definitely different from the larger ones. To the best of our knowledge, this is the first observation of a 154CVE cluster.

If we consider the Pt_{12} cluster to be less symmetric C_{2v}, we could explain such an exceptionally high ORR activity from the theoretical analysis of the oxygen adsorption energy (Figure 6). Many previous results of the ORR catalysis exhibited a good correlation between the activity and the binding energy of an oxygen atom on the $Pt(111)$ surface, especially known as a "volcano-shape" relationship.[30−32] Based on this analysis, an estimated ORR activity of the icosahedral Pt_{13} cluster was very low because the binding energy (ΔE_0) is too strong (-1.0 eV for bulk Pt) to recover the reduced surface.[33] In sharp contrast, ΔE_0 of the $Pt_{12}(C_{2v})$ cluster (0.2−0.3 eV) is ideal. This might be one of the primary reasons for the improved ORR catalytic activity by the Pt_{12} cluster. In practice, we should consider the presence of surface coordinating ligands (dendrimers), some minor structural isomers,[27] and counting of the inaccessible sites[30] for the quantitative discussion.

DISCUSSION

The "size effect" issue is now reexamined. Smaller platinum clusters have been believed to be less active for the ORR. This has been explained as a result of the too strong Pt−O binding on the smaller cluster.[3] Accordingly, reduction of the size from that of larger Pt nanoparticles having a face-centered-cubic (FCC) structure ($\sim$3 nm) will increase the Pt−O binding energy, which may lead to a loss in the ORR activity. However, the previous and present results suggest that the internal structure would change to icosahedral if the cluster size approached 1 nm (ca. 20−30 atoms).[34] Furthermore, the second structural transition to the less symmetrical structure would be caused by a size reduction beyond the smallest limit of the icosahedral clusters (Pt_{13}), reawakening the catalytic activity. There are several examples reporting that the structural distortion,[35] shape conversion,[7] or appearance of high-order facets can provide enhanced ORR activity.[36] Interestingly, such a distortion-induced enhancement of the catalytic activity was also found in the natural photosynthetic system.[37]

CONCLUSION

We successfully synthesized platinum clusters having a definite number of metal atoms by chemical stoichiometric control. This is the first observation that the as-synthesized clusters have atomic-level precision, which does not rely on the inherent stability occasionally found in magic number clusters. The primary significance of our approach is that even clusters that deviated from the magic number (e.g., Pt_{12}) can be precisely synthesized. This synthetic breakthrough allowed us to find a hidden catalytic performance of these metastable clusters. In

particular, Pt_{12} has catalytic activity about 2.5-fold higher than that of Pt_{13} for the ORR and also has an activity much higher than that of the larger clusters (Pt_{28} or Pt_{60}). At the same time, the low activity of Pt_{13} adequately explains the commonly observed size dependence that smaller clusters around 1 nm have versus the lower ORR activity. Therefore, the present results support the idea that such a simple relationship between the size and the activity no longer exists on a subnanometer scale. This idea also suggests that catalysts having exceptionally high activity can be produced by the deformation of subnanometer clusters with a specific number of metal atoms.

ASSOCIATED CONTENT

S Supporting Information

Detailed experimental and analytical methods, synthesis and characterization of the materials, and experimental data including RDV, ESI-TOF-MS, XAFS and DFT calculation. This material is available free of charge via the Internet at http://pubs.acs.org.

AUTHOR INFORMATION

Corresponding Author
yamamoto@res.titech.ac.jp

Author Contributions

The manuscript was written through the contributions of all authors. All authors have given approval to the final version of the manuscript.

Notes

The authors declare no competing financial interest.

REFERENCES

(1) (a) Astruc, D., Ed. *Nanoparticles and Catalysis*; Wiley-VCH: Weinheim, Germany, 2008. (b) Raimondi, F.; Scherer, G. G.; Körz, R.; Wokaun, A. *Angew. Chem., Int. Ed.* **2005**, *44*, 2190−2209. (c) Astruc, D.; Lu, F.; Aranzaes, J. R. *Angew. Chem., Int. Ed.* **2005**, *44*, 7852−7872.

(2) (a) Kinoshita, K. *J. Electrochem. Soc.* **1990**, *137*, 845−848. (b) Mayrhofer, K.; Blizanac, B.; Arenz, M.; Stamenkovic, V. R.; Ross, P. N.; Markovic, N. M. *J. Phys. Chem. B* **2005**, *109*, 14433−14440. (c) Nesselberger, M.; Ashton, S.; Meier, J. C.; Katsounaros, I.; Mayrhofer, K. J. J.; Arenz, M. *J. Am. Chem. Soc.* **2011**, *133*, 17428−17433. (d) Debe, M. K. *Nature* **2013**, *486*, 43−51.

(3) Shao, M.; Peles, A.; Shoemaker, K. *Nano Lett.* **2011**, *11*, 3714−3719.

(4) Yano, H.; Inukai, J.; Uchida, H.; Watanabe, M.; Babu, P. K.; Kobayashi, T.; Chung, J. H.; Oldfield, E.; Wieckowski, A. *Phys. Chem. Chem. Phys.* **2006**, *8*, 4932−4939.

(5) Yamamoto, K.; Imaoka, T.; Chun, W.-J.; Enoki, O.; Katoh, H.; Takenaga, M.; Sonoi, A. *Nat. Chem.* **2009**, *1*, 397−402.

(6) (a) Gotoh, K.; Hashimoto, H.; Kawai, R.; Nishina, Y.; Fujii, E.; Ohkubo, T.; Itadani, A.; Kuroda, Y.; Ishida, H. *Chem. Lett.* **2012**, *41*, 680−682. (b) Bruix, A.; Rodriguez, J. A.; Ramírez, P. J.; Senanayake, S. D.; Evans, J.; Park, J. B.; Stacchiola, D.; Liu, P.; Hrbek, J.; Illas, F. *J. Am.*

Chem. Soc. **2012**, *134*, 8968−8974. (c) Dong, Q.; Li, G.; Ho, C.-L.; Faisal, M.; Leung, C.-H.; Pong, P. W.-T.; Liu, K.; Tang, B.-Z.; Manners, I.; Wong, W.-Y. *Adv. Mater.* **2012**, *24*, 1034−1040. (d) Liang, Y.; Li, Y.; Wang, H.; Dai, H. *J. Am. Chem. Soc.* **2013**, *135*, 2013−2036.

(7) Mostafa, S.; Behafarid, F.; Croy, J. R.; Ono, L. K.; Li, L.; Yang, J. C.; Frenkel, A. I.; Cuenya, B. R. *J. Am. Chem. Soc.* **2010**, *132*, 15714−15719.

(8) (a) Eberhardt, W.; Fayet, P.; Cox, D. M.; Fu, Z.; Kaldor, A.; Sherwood, R.; Sondericker, D. *Phys. Rev. Lett.* **1990**, *64*, 780−783. (b) Yasumatsu, H.; Hayakawa, T.; Koizumi, S.; Kondow, T. *J. Chem. Phys.* **2005**, *123*, 124709.

(9) (a) Femoni, C.; Kaswalder, F.; Iapalucci, M. C.; Longoni, G.; Mehlstäubl, M.; Zacchini, S.; Ceriotti, A. *Angew. Chem., Int. Ed.* **2006**, *45*, 2060−2062. (b) Femoni, C.; Iapalucci, M. C.; Longoni, G.; Wolowska, J.; Zacchini, S.; Zanello, P.; Fedi, S.; Riccò, M.; Pontiroli, D.; Mazzani, M. *J. Am. Chem. Soc.* **2010**, *132*, 2919−2927. (c) Roth, J. D.; Lewis, G. J.; Safford, L. K.; Jiang, X. D.; Dahl, L. F.; Weaver, M. J. *J. Am. Chem. Soc.* **1992**, *114*, 6159−6169. (d) Washecheck, D. M.; Wucherer, E. J.; Dahl, L. F.; Ceriotti, A.; Longoni, G.; Manassero, M.; Sansoni, M.; Chini, P. *J. Am. Chem. Soc.* **1979**, *101*, 6110−6112.

(10) Femoni, C.; Iapalucci, M. C.; Longoni, G.; Zacchini, S.; Zarra, S. *J. Am. Chem. Soc.* **2011**, *133*, 2406−2409.

(11) (a) Tomalia, D. A. *Soft Matter* **2010**, *6*, 456. (b) Bronstein, L. M.; Shifrina, Z. B. *Chem. Rev.* **2011**, *111*, 5301−5344. (c) Ye, H.; Crooks, R. M. *J. Am. Chem. Soc.* **2005**, *127*, 4877−4873.

(12) (a) Nakamula, I.; Yamanoi, Y.; Imaoka, T.; Yamamoto, K.; Nishihara, H. *Angew. Chem., Int. Ed.* **2011**, *50*, 5830−5833. (b) Nakamula, I.; Yamanoi, Y.; Yonezawa, T.; Imaoka, T.; Yamamoto, K.; Nishihara, H. *Chem. Commun.* **2008**, 5716−5718. (c) Satoh, N.; Nakashima, T.; Kamikura, K.; Yamamoto, K. *Nat. Nanotechnol.* **2008**, *3*, 106−111.

(13) (a) Yamamoto, K.; Higuchi, M.; Shiki, S.; Tsuruta, M.; Chiba, H. *Nature* **2002**, *415*, 509−511. (b) Yamamoto, K.; Imaoka, T. *Bull. Chem. Soc. Jpn.* **2006**, *79*, 511−526.

(14) Enoki, O.; Katoh, H.; Yamamoto, K. *Org. Lett.* **2006**, *8*, 569−571.

(15) Kitazawa, H.; Albrecht, K.; Yamamoto, K. *Chem. Lett.* **2012**, *41*, 828−830.

(16) Zhang, B.; Zhang, W.; Su, D. S. *ChemCatChem* **2011**, *3*, 965−968.

(17) Negishi, Y.; Chaki, N. K.; Shichibu, Y.; Whetten, R. L.; Tsukuda, T. *J. Am. Chem. Soc.* **2007**, *129*, 11322−11323.

(18) Tanaka, S.-I.; Miyazaki, J.; Tiwari, D. K.; Jin, T.; Inouye, Y. *Angew. Chem., Int. Ed.* **2011**, *50*, 431−435.

(19) (a) Akdogan, Y.; Anantharaman, S.; Liu, X.; Lahiri, G. K.; Bertagnolli, H.; Roduner, E. *J. Phys. Chem. C* **2009**, *113*, 2352−2359. (b) Jupally, V. R.; Kota, R.; Dornshuld, E. V.; Mattern, D. L.; Tschumper, G. S.; Jiang, D.; Dass, A. *J. Am. Chem. Soc.* **2011**, *133*, 20258−20266.

(20) Longoni, G.; Chini, P. *J. Am. Chem. Soc.* **1976**, *98*, 7225−7231.

(21) Butcher, C. P. G.; Dyson, P. J.; Johnson, B. F. G.; Khimyak, T.; McIndoe, J. S. *Chem.—Eur. J.* **2003**, *9*, 944−950.

(22) Johansson, M. P.; Pyykkö, P. *Chem. Commun.* **2010**, *46*, 3762.

(23) Mingos, D. M. P. *J. Chem. Soc., Chem. Commun.* **1985**, 1352.

(24) Russell, A. E.; Rose, A. *Chem. Rev.* **2004**, *104*, 4613−4635.

(25) Frenkel, A. I.; Hills, C. W.; Nuzzo, R. G. *J. Phys. Chem. B* **2001**, *105*, 12689−12703.

(26) Alexeev, O. S.; Siani, A.; Lafaye, G.; Williams, C. T.; Ploehn, H. J.; Amiridis, M. D. *J. Phys. Chem. B* **2006**, *110*, 24903−24914.

(27) Häkkinen, H. *Chem. Soc. Rev.* **2008**, *37*, 1847−1859.

(28) Mingos, D. M. P. *Acc. Chem. Res.* **1984**, *17*, 311−319.

(29) (a) de Silva, N.; Dahl, L. F. *Inorg. Chem.* **2005**, *44*, 9604−9606. (b) Kurasov, S. S.; Eremenko, N. K.; Slovokhotov, Y. L.; Struchkov, Y. T. *J. Organomet. Chem.* **1989**, *361*, 405−408.

(30) Friebel, D.; Viswanathan, V.; Miller, D. J.; Anniyev, T.; Ogasawara, H.; Larsen, A. H.; O'rady, C. P.; Nørskov, J. K.; Nilsson, A. *J. Am. Chem. Soc.* **2012**, *134*, 9664−9671.

(31) Greeley, J.; Stephens, I. E. L.; Bondarenko, A. S.; Johansson, T. P.; Hansen, H. A.; Jaramillo, T. F.; Rossmeisl, J.; Chorkendorff, I.; Nørskov, J. K. *Nat. Chem.* **2009**, *1*, 552−556.

(32) (a) Stamenkovic, V.; Mun, B. S.; Mayrhofer, K. J. J.; Ross, P. N.; Markovic, N. M.; Rossmeisl, J.; Greeley, J.; Nørskov, J. K. *Angew. Chem., Int. Ed.* **2006**, *45*, 2897−2901. (b) Zhang, J.; Vukmirovic, M. B.; Xu, Y.; Mavrikakis, M.; Adzic, R. R. *Angew. Chem., Int. Ed.* **2005**, *44*, 2132−2135.

(33) Markovic, N. M.; Ross, P. N. *Surf. Sci. Rep.* **2002**, *45*, 121−229.

(34) (a) Rodriguez, A.; Amiens, C.; Chaudret, B.; Casanove, M.-J.; Lecante, P.; Bradley, J. S. *Chem. Mater.* **1996**, *8*, 1978−1986. (b) Barreteau, C.; Desjonquères, M. C.; Spanjaard, D. *Eur. Phys. J. D* **2000**, *11*, 395−402.

(35) (a) Wang, J. X.; Ma, C.; Choi, Y.; Su, D.; Zhu, Y.; Liu, P.; Si, R.; Vukmirovic, M. B.; Zhang, Y.; Adzic, R. R. *J. Am. Chem. Soc.* **2011**, *133*, 13551−13557. (b) Strasser, P.; Koh, S.; Anniyev, T.; Greeley, J.; More, K.; Yu, C.; Liu, Z.; Kaya, S.; Nordlund, D.; Ogasawara, H.; Toney, M. F.; Nilsson, A. *Nat. Chem.* **2010**, *2*, 454−460.

(36) (a) Lim, B.; Jiang, M.; Camargo, P. H. C.; Cho, E. C.; Tao, J.; Lu, X.; Zhu, Y.; Xia, Y. *Science* **2009**, *324*, 1302−1305. (b) Tian, N.; Zhou, Z.-Y.; Sun, S.-G.; Ding, Y.; Wang, Z. L. *Science* **2007**, *316*, 732−735.

(37) Umena, Y.; Kawakami, K.; Shen, J.-R.; Kamiya, N. *Nature* **2012**, *473*, 55−60.

13095

dx.doi.org/10.1021/ja405922m | *J. Am. Chem. Soc.* 2013, 135, 13089−13095